Experimental and Theoretical Investigations of Turbulent Flow in a Side-Inlet Rectangular Combustor

T.-M. Liou,* S.-M. Wu,† and Y.-H. Hwang†
National Tsing Hua University, Hsin-Chu, Taiwan, Republic of China

Experimental and theoretical studies are reported on a turbulent flow in a side-inlet rectangular combustor with an aspect ratio of 4:1. A laser-Doppler velocimeter was used to measure the axial and transverse mean velocity and turbulence intensity components as well as Reynolds stress and turbulent kinetic energy. The Reynolds numbers based on the air density, combustor hydraulic diameter, and bulk velocity were in the range of 1.0×10^3 to 2.0×10^5. The governing partial differential equations were solved numerically with the two-equation k-ϵ turbulence model. Reasonable agreement is demonstrated between the measured and calculated mean-velocity profiles. Flow oscillations are determined from the measured velocity probability density functions. Regions where turbulence is anisotropic and where turbulent kinetic energy and shear stresses dominate are identified. In addition, the effects of the dome height on the impinging stagnation point, the reattachment lengths, and the fractions of the inlet mass flow rate transported into the dome recirculation region and the secondary recirculation regions, respectively, are investigated. Furthermore, the variation of the reattachment length with the Reynolds number and the spanwise flow distribution presented in this study are believed to be a useful test of the combustor modeling.

Nomenclature

B = inlet-duct width, mm
c_1, c_2, c_μ = constants in turbulence model
D_C = combustor transverse length, mm
D_H = combustor hydraulic diameter, mm
k = turbulent kinetic energy, m^2/s^2
L_D = dome height, mm
ℓ = turbulence length scale
$\dot{m}_1$ = mass flow rate of dome zone
$\dot{m}_2$ = mass flow rate of secondary recirculation zone
Re_C = combustor Reynolds number, $\equiv \rho U_{REF} D_H / \mu_l$
S_ϕ = source term of the dependent variables ϕ
U = axial mean velocity, m/s
U_{REF} = combustor bulk mean velocity, m/s
u' = axial turbulence intensity, m/s
V = transverse mean velocity, m/s
v' = transverse turbulence intensity, m/s
X = combustor axial coordinate, mm
X^* = normalized combustor axial coordinate, $X \geq 0$: $X^* \equiv X/D_C$; $X < 0$: $X^* \equiv X/L_D$
Y = combustor transverse coordinate, mm
Y^* = normalized combustor transverse coordinate, $\equiv Y/(D_C/2)$
Z = combustor spanwise coordinate, mm
Z_C = combustor spanwise width, mm
Z^* = normalized combustor spanwise coordinate, $\equiv Z/(Z_C/2)$
λ = dimensionless inlet turbulence length scale
ρ = air density, kg/m^3
ϕ = dependent variables of the P.D.E.'s equations
τ_ϕ = turbulent diffusion coefficient of dependent variables ϕ
ϵ = turbulent dissipation rate
μ_l = molecular viscosity, kg/m-s
μ_t = turbulence viscosity, kg/m-s

Received April 12, 1988; revision received Dec. 2, 1988.

*Professor, Power Mechanical Engineering Department.
†Graduate Student, Power Mechanical Engineering Department.

Introduction

SIDE-DUMP combustors are being investigated as a possible alternative to coaxial-dump combustors for a light and compact propulsion system. In a side-dump combustor, two or more jets are introduced through ports in the combustor periphery. The enhanced mixing and large-scale recirculation, which are conducive to easy ignition and anchorage for the flame, occur in a complex flowfield formed by the impingement of these jets. Therefore, a better understanding of the fluid dynamic processes involved in such a combustor is necessary for improving the flame stabilization and combustion efficiency.

In contrast to the coaxial-dump combustors, there have been very few studies of the detailed flow structure inside the side-dump combustors. Shahaf et al.[1] studied a two-dimensional side-dump square combustor model of a liquid-fueled ramjet both analytically and experimentally. The results relevant to the flowfield were presented in terms of axial mean velocity only and were measured at a few axial stations. They concluded that a 90-deg inlet angle gave the best overall performance. Stull et al.[2] and Vanka et al.[3] investigated analytically the flowfield characteristics of a three-dimensional side-inlet dump combustor by varying the positions of the dome plate and the angle of the side inlets. However, neither of them provided information relevant to turbulence. Vanka et al.[4] further performed preliminary calculations of the three-dimensional reacting flowfield in a side-dump combustor with gaseous fuel injected through the dome plate and air induced through two 45-deg inlet ducts. Their results were reported in terms of mean flow patterns, temperature and fuel fraction distributions, and combustion efficiency. Unfortunately, there are no experimental data to validate the turbulence and combustion models used in their calculations. In addition to the aforementioned computations, flow visualization is a useful method for qualitatively revealing the flow structures. Using the hydrogen-bubble technique and a water channel, Nosseir and Behar[5] investigated the periodic phenomena associated with the impingement of the two counterdirectional inlet jets. They observed that the streamwise vortices formed in the impinging region were directly related to the velocity modulations in the two inlet flows. Recently, Miau and Sun[6] per-

formed a similar study in a side-inlet square duct using the particle-tracer visualization technique. Their results supported the observation made by Nosseir and Behar. In view of the lack of quantitative experimental data, particularly the turbulence data, with which to compare numerical predictions, Liou and Wu performed detailed mean-velocity and turbulence intensity measurements in curved 60-deg inlet ducts[7] and in a three-dimensional side-dump combustor with a circular cross section[8] using laser-Doppler velocimetry (LDV); however, their measurements were carried out at a single Reynolds number only.

The present study has been undertaken to both experimentally and analytically investigate the cold flowfield in a side-dump rectangular combustor. A combustor with a rectangular cross section was chosen since it allowed us to use the measured data to validate our two-dimensional computer code. The side inlets were designed to intersect the combustor walls at an angle of 90 deg due to its better overall performance, as reported by Shahaf et al.[1] The measurements were made using LDV, since the flow reversal in the dome recirculation region and the large turbulence fluctuations generated by the jet-to-jet impingement make the use of hot-wire technique impractical. Furthermore, the brief literature survey made above points out that turbulence information is lacking, and this fact has encouraged the authors to characterize the flowfield in terms of mean velocity, turbulence intensity, Reynolds stress, and turbulent kinetic energy. Also, the Reynolds number and the dome height were varied to study their influences on the various flow characteristics. It is hoped that the results presented in this study will provide useful information to the designers.

Experimental Apparatus and Conditions

The dual-inlet-side-dump combustor and LDV experimental setup were shown schematically and described in detail in Ref. 8. The major differences between the present work and Ref. 8 are the configuration of the combustion chamber and the experimental conditions that are described in the following.

Combustion Chamber Model

The configuration of the dual-inlet side-dump combustor model, coordinate system, and dimensions are presented in Fig. 1. The combustor model consisted of two short rectangular inlet ducts and a rectangular chamber.

The two 20-mm-long rectangular inlet ducts intersected the combustor at an angle of 90 deg and were separated azimuthally by 180 deg. The internal dimensions ($X \times Z$) of the inlet ducts were 15×120 mm^2. The upstream edge of the inlet ports was taken as the combustor axial zero reference point and, thus, the axial coordinate downstream of the zero reference point was positive.

The combustor model was made of 5-mm-thick Plexiglas. It had an adjustable flat dome plate. The combustor duct had a cross-sectional area of 30×120 mm and was 2000 mm long from the axial zero reference point to the exit. No exit nozzle was used in this experiment.

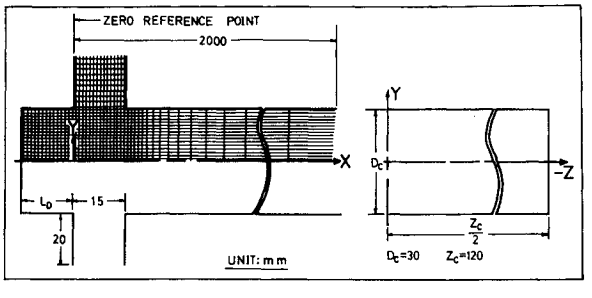

Fig. 1 Sketch of configuration, coordinate system, dimensions, and computational grids of the combustor.

Experimental Conditions

For the inlet ducts, the velocity measurements were made at four stations, i.e., $Y^* = \pm 1$ and ± 2. For the combustion chamber, the measurements were made at 11 stations normal to the combustor axis. These X^* stations were located at $X^* = -0.6$, 0.0, 0.25, 0.5, 0.72, 1.1, 1.6, 2.5, 4.0, 9.0, and 15.0, respectively. In each station, the measurements were made at locations 13–15 along the central plane ($Z^* = 0.0$) or locations 117–135 over the whole (Y^*-Z^*) plane. A combustor bulk velocity of 13.4 m/s was used as a reference to normalize the experimental results. The Reynolds number Re_C, based on combustor hydraulic diameter and bulk velocity, was 4.1×10^4, indicating that the flow was turbulent. The ratio of dome height to combustor height (L_D/D_C) was 0.5. In addition to the above referenced case, the Reynolds number was varied between 1.0×10^3 to 2.0×10^5 in this study. Also, the normalized dome height L_D/D_C was varied from 0 to 4 to study its effect on the various characteristic parameters.

Theoretical Prediction

Prediction of the fluid flow in a side-dump rectangular combustor was obtained by numerically solving the governing elliptic differential equations. To simplify the complicated problem, the cold flow was considered to be incompressible, two-dimensional, and steady-state.

Governing Equations

The general form of the governing equations is

$$\left[\frac{\partial}{\partial X}(\rho U\phi)+\frac{\partial}{\partial Y}(\rho V\phi)\right]-\left[\frac{\partial}{\partial X}\left(\tau_\phi\frac{\partial\phi}{\partial X}\right)+\frac{\partial}{\partial Y}\left(\tau_\phi\frac{\partial\phi}{\partial Y}\right)\right]=S_\phi$$

where ϕ, τ_ϕ, and S_ϕ are specified in Table 1. The two-equation k-ϵ turbulence model was employed to specify the turbulence viscosity (μ_t) appearing in the momentum equations. According to this model,

$$\mu_{\text{eff}} = \mu_l + \mu_t \qquad \text{and} \qquad \mu_t = c_\mu \rho k^2/\epsilon$$

It should be noted that μ_t is assumed to be isotropic in the model k and ϵ in the above equation are obtained by solving the k-equation and the ϵ-equation, as given in Table 1. The associated empirical constants such as σ_k, σ_ϵ, c_1, c_2, and c_μ are 1.0, 1.3, 1.44, 1.92, and 0.09, respectively.[9]

Table 1 Dependent variables and their corresponding turbulent diffusion coefficients and source terms in the governing equations

Conservation equation	ϕ	τ_ϕ	S_ϕ
Mass	1	0	0
X momentum	U	μ_{eff}	$-\frac{\partial P}{\partial X}+S^u$
Y momentum	V	μ_{eff}	$-\frac{\partial P}{\partial Y}+S^v$
Turbulent kinetic energy	k	$\mu_l+\frac{\mu_t}{\sigma_k}$	$G-\rho\epsilon$
Turbulent dissipation rate	ϵ	$\mu_l+\frac{\mu_t}{\sigma_\epsilon}$	$(c_1\epsilon G-c_2\rho\epsilon^2)\frac{1}{k}$

$$S^u=\frac{\partial}{\partial X}\left(\mu_{\text{eff}}\frac{\partial U}{\partial X}\right)+\frac{\partial}{\partial Y}\left(\mu_{\text{eff}}\frac{\partial U}{\partial Y}\right)$$

$$S^v=\frac{\partial}{\partial X}\left(\mu_{\text{eff}}\frac{\partial V}{\partial X}\right)+\frac{\partial}{\partial Y}\left(\mu_{\text{eff}}\frac{\partial V}{\partial Y}\right)$$

$$G=\mu_t\left[2\left(\frac{\partial U}{\partial X}\right)^2+2\left(\frac{\partial V}{\partial Y}\right)^2+\left(\frac{\partial U}{\partial Y}+\frac{\partial V}{\partial X}\right)^2\right]$$

Boundary Conditions

The above set of partial differential equations has to be solved with the following boundary conditions:

1) Symmetric axis ($Y^* = 0$)

$$\frac{\partial \phi}{\partial Y} = 0, \qquad V = 0 \qquad \text{where} \qquad \phi = U, k, \epsilon$$

2) Inlet

$$U = U_{in} \approx 0, \qquad V = V_{in} \qquad \text{and} \qquad k = k_{in}$$

measured at $Y^* = \pm 2$

$$\epsilon = \epsilon_{in} = k_{in}^{3/2}/\ell = k_{in}^{3/2}/(B\lambda)$$

where $B = D_C/2, \qquad \lambda = 0.005$

The turbulence length scale ℓ is determined by the characteristic mesh size of the screens in the settling chamber and by the 10:1 contraction of bell-mouth entry that is situated upstream of each side inlet duct[8]; the dimensionless turbulence scale λ is normalized by inlet-duct width. Note that the computed results are found to be insensitive to λ ranged from 0.001 to 0.01.

3) Exit

$$\frac{\partial \phi}{\partial X} = 0, \qquad V = 0, \qquad \text{where} \qquad \phi = U, k, \epsilon$$

In this study, the downstream boundary is set at $X^* = 9$, which is determined from the measured results as will be discussed later.

4) Walls

$$U = 0, \qquad V = 0$$

Since the k-ϵ model is valid only in those flow regions that are strongly turbulent, i.e., in regions where the eddy diffusivity μ_t overwhelms the molecular diffusivity μ_t, it does not apply in the viscous sublayer. In this study, the near-wall region was simulated by the two-zone model, i.e., viscous sublayer and fully turbulent zone, and the wall-function method[9] was used to bridge the viscous sublayer.

Numerical Scheme

The solution of the partial differential equations along with the boundary conditions was obtained by using a finite-difference scheme based on the SIMPLE solution algorithm of Patankar and Spalding.[10] The solution procedure starts by supplying initial guesses for the velocity and pressure fields and then proceeds the line-by-line iteration.[10] After each sweep over the solution domain, adjustments for the pressure field are made to satisfy the continuity along each line of cells. These adjustments, in turn, destroy the compliance of the velocity and pressure field with the momentum equations. Further iterations are thus needed until the continuity and momentum equations are simultaneously satisfied to the requisite degree of accuracy. The tolerances of the mass and momentum residuals nondimensionalized by their corresponding inlet flux are typically 0.005 to 0.0001. The k and ϵ equations are also solved line by line simultaneously with the mean-velocity distribution.

A grid refinement test showed that the computational results for the 55 × 28 grid are almost identical to those for a 65 × 52 grid. The calculations of this study then were made using a 55 × 28 grid (Fig. 1) in the axial and transverse direction, respectively. A large number of grid points were placed in the areas where steep variation in velocities were revealed from experimental measurements. Typically, the convergence needs 400 to 600 iterations. The corresponding CPU times on a CDC-CYBER 180/840 computer are 450 to 1000 s.

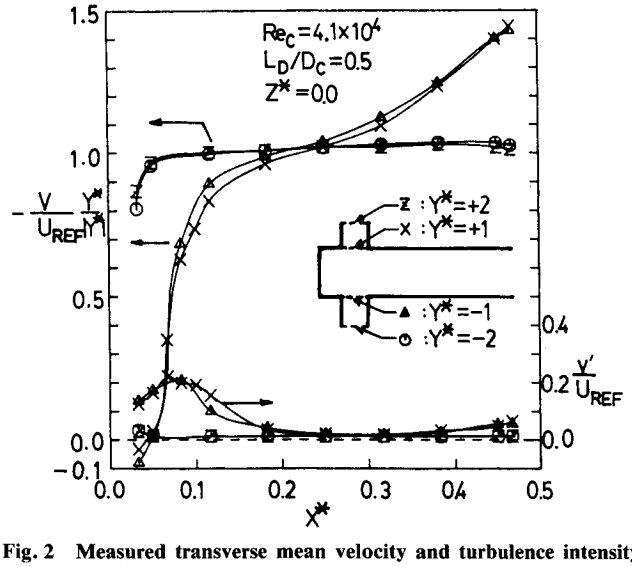

Fig. 2 Measured transverse mean velocity and turbulence intensity profiles at $Y^* = \pm 1$ and ± 2.

Results and Discussion

Data Accuracy

The mean velocity and turbulence intensity were calculated from the probability density function (PDF) of the measurements.[8] There were typically 4000 measurements at each measuring location. The corresponding statistical error was between 0.04 and 1.31% in the mean velocity and between 2.2 and 3.1% in the turbulence intensity for the 95% confidence level. The error in U_{REF} was ±1%.

Various weighting methods have been proposed to correct the velocity bias effect,[11,12] but none of these is entirely satisfactory. They all involve assumptions regarding the statistical distribution of particles in the flow. The weighting method proposed by McLaughlin and Tiederman,[13] in which the weighting factor is simply the inverse of the velocity or the particle residence time, has been widely used because of its simplicity. This scheme was therefore used in this study for regions where the turbulence level was below 30%. The difference between weighted and unweighted data sets was found to be relatively small (below 1.5%). In regions where the turbulence level was larger than 30%, this weighting scheme is not totally suitable for the present experiment[11]; however, a few measurements at representative points were repeated using equal time interval averaging, and the error due to velocity bias was found to be within 4.2%.

The position accuracy was limited by the milling machine[8] and by the finite size of the LDV probe volume. The errors in the axial, transverse, and spanwise positions were approximately ±0.3, ±0.3, and ±0.5 mm, respectively.

Flow Distribution in the Inlet Ducts

Figure 2 shows the measured transverse mean velocity (V/U_{REF}) and turbulence intensity (v'/U_{REF}) profiles for $Y^* = \pm 1$ and $Y^* = \pm 2$. The 10:1 contraction provided a uniform profile for both V/U_{REF} and v'/U_{REF} at $Y^* = \pm 2$. A deviation from the uniform profile occurs near $X^* = 0.03$ where the flow is retarded by the low-velocity flow (Fig. 3) in the dome region. This retardation is increased as the flow proceeds toward the dump plane ($Y^* = \pm 1$) where the flow even separates near $X^* = 0.03$. A similar result was also found for the curved inlet duct flow of a three-dimensional side-inlet dump combustor.[7] The retardation leads to a very steep mean-velocity gradient in the region of $0 < X^* < 0.15$ and, in turn, an increase in the corresponding turbulence intensity.

The velocity profiles in Fig. 2 at $Y^* = +2$ and $Y^* = +1$ are almost the same as those at $Y^* = -2$ and $Y^* = -1$, respectively. The difference is within 0.2% for $Y^* = \pm 2$ and within 2.0% for $Y^* = \pm 1$. The two nearly identical inlet flows then are dumped into the combustion chamber.

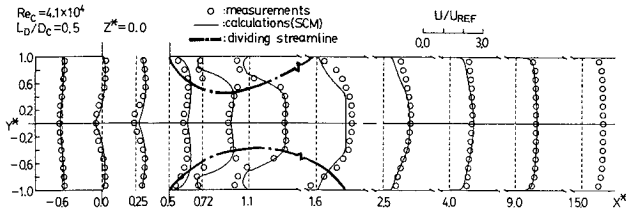

Fig. 3 Measured and calculated mean axial velocity.

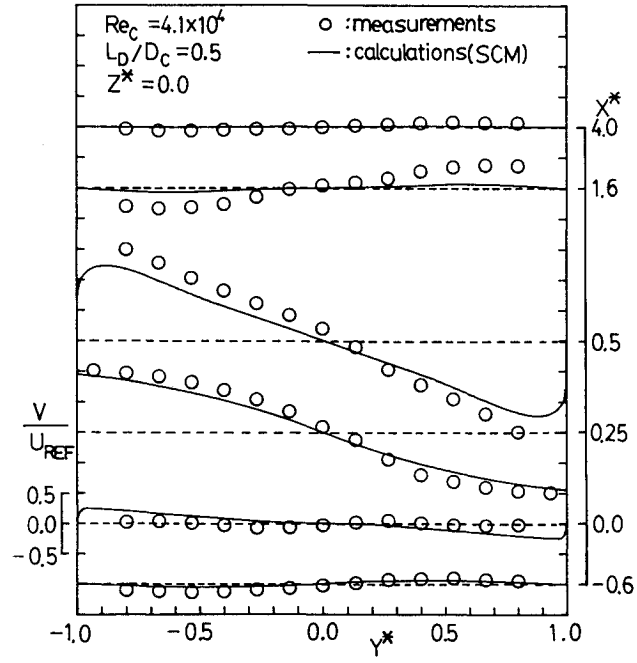

Fig. 4 Measured and calculated mean transverse velocity profiles.

Mean-Velocity Characteristics in the Combustor

Figure 3 shows the measured and predicted mean axial velocity profiles throughout the side-dump combustor flowfield. As one can see, the centerline velocity varies significantly from $X^* = 0.25$ to 0.5, since the impinging dividing streamline of the two inlet jets lies within this axial interval. Note that the impinging stagnation point occurs at $X^* = 0.28$ and $Y^* = 0.0$, which is identified by moving the LDV probe volume between $X^* = 0.25$ and 0.5 along the combustor axis. Furthermore, two pairs of counter-rotating vortices are driven by the sudden expansion of the inlet flow, by the shear of the jet, and by the spread of the impinging jets. One of the two pairs of vortices is located between the impinging dividing streamline and the dome plate. Also note that the mean axial velocity in the dome region is smaller than those of other regions in the combustor. This low velocity ensures ready anchorage for the flame. The other pair of counter-rotating vortices is located immediately downstream of the impinging dividing streamline on the side walls, where the two inlet jets separate from the downstream edges ($X^* = 0.5$, $Y^* = \pm 1.0$) of the inlet ports and reattach to the walls at points ($X^* = 1.43$, $Y^* = 1.0$) and ($X^* = 1.73$, $Y^* = -1.0$), respectively. The difference between the two reattachment lengths reveals the slight asymmety of the two recirculation zones. In this study, we shall call these two zones the secondary recirculation zones.

Figure 3 shows that the downstream flow at $X^* > 2.5$ redevelops and gradually becomes fully developed. A comparison of the mean axial velocity profiles between $X^* = 9.0$ and 15.0 shows that the difference is very small (within 0.3%). Hence, $X^* = 9.0$ was chosen as the downstream boundary of the computing domain, where the axial gradients of the dependent variables are often assumed to vanish. In fact, the flow moves unidirectionally downstream for $X^* \geq 4$.

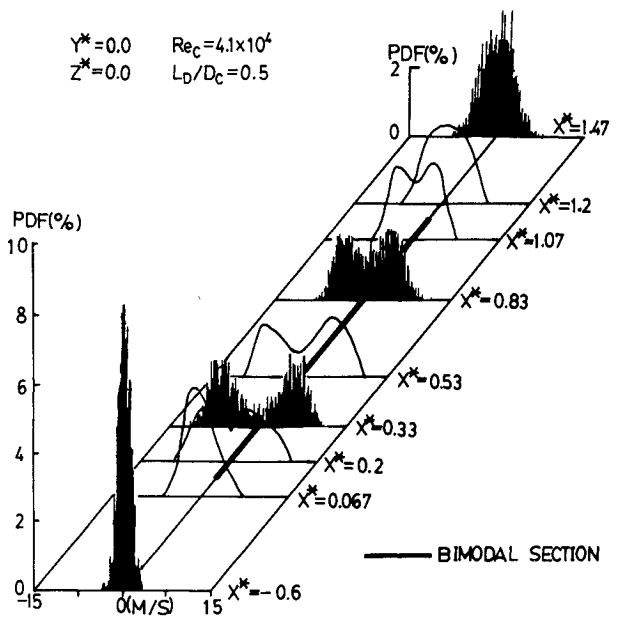

Fig. 5 Axial variations in the PDF of measured transverse velocity along the centerline.

The comparison between the predicted and measured mean axial velocity profiles at various X^* shows that the agreement is reasonably good. Additionally, since the flowfield in the region of $-0.6 \leq X^* < 1.6$ (Fig. 3) involves jet impingement and recirculating flow, the inlet jets in this region undergo considerable deflection, from quasiperpendicular to quasiparallel to the combustor axis. Thus, the streamline curvature modification (SCM) proposed by Leschziner and Rodi[14] was applied to the present computations. Note that the calculated results for $-1 \leq Y^* \leq 0$ are identical to those for $0 \leq Y^* \leq 1$ since the computation is based on the assumption of symmetry with respect to combustor axis.

The measured and predicted mean transverse velocity profiles at various X^* are plotted in Fig. 4. Reasonable agreement is obtained. The large velocities in the region of $0 \leq X^* \leq 0.5$ indicate the inlet jets. In addition, the near-zero transverse mean velocity at the centerline ($Y^* = 0$) shows that the two jets impinge on each other. In the dome region ($X^* \leq 0$) the mean transverse velocity is found to be quite low. Note that the low mean transverse velocity in the dome region is consistent with the observation made previously for the mean axial velocity. Moreover, the zero transverse mean velocity downstream of $X^* = 4$ suggests that the flow is unidirectional for $X^* \geq 4$. Figures 5 and 6a show the axial and transverse variations of measured transverse velocity PDF in the jet impingement region, respectively. Along the centerline (Fig. 5) all the PDF's display the presence of both positive and negative instantaneous velocities. The PDF becomes bimodal for $0.1 \leq X^* \leq 1.1$. These observations illustrate hte presence of a fluctuation in the dome recirculation pattern and a variation in the position of the side-inlet jet interaction region. The large-scale flow oscillations then can be schematically expressed as Fig. 6b, which also can be observed qualitatively using instantaneous water flow visualization at different times during the same test, as done by Kennedy[15] and Nosseir and Behar[5] in similar combustor configurations.

The transverse variations in the velocity PDF (Fig. 6a) reveal how deep the flow oscillations penetrate into the Y^* direction. When large-scale oscillations in the flowfield occur, it was reported that the mass flow into the dome recirculation region increases significantly, and the residence time in the recirculation region decreases significantly.[15] Thus, the flow oscillations have relevance to the flame stabilization characteristics of the dome recirculation.

Turbulence Intensity

Figure 7 shows profiles of both the measured axial and transverse turbulence intensities. Peak values of the transverse turbulence intensity occur in the region of jet impinging and reach a value as high as 42.4% near the centerline, where the velocity PDF's have bimodal distributions, as shown earlier in Figs. 5 and 6. Furthermore, both axial and transverse turbulence intensities have peak values occurring around the reattachments and in the shear layers of the secondary recirculation zones, e.g., at ($X^* = 1.1$, $Y^* = -0.533$), (1.1, −0.667), (1.1, 0.667), (1.6, −0.8), and (1.6, 0.933), where large gradients of the mean velocity prevail. The axial turbulence intensity reaches a maximum value of 62.0%. It is interesting to note that the peak transverse turbulence intensity is approximately two-thirds the value of the peak axial turbulence intensity. This behavior is also found in free jet flow, as shown by Wygnanski and Fiedler.[16]

The difference between the axial and transverse turbulence intensities in Fig. 7 is rather large in the jet impinging region and in the shear layers of the secondary recirculation zones. Hence, the turbulence is rather anisotropic in these regions. In fact, the anisotropy of turbulence in the aforementioned regions is associated with the nature of the large-scale motion observed in Figs. 5 and 6, since the mean motion usually has preferred directions that are imposed on the large-scale turbulent motion. The anisotropic turbulence found in the present study also suggests that the isotropic eddy viscosity assumption, i.e., the eddy viscosity is the same for all turbulence stresses, used in the k-ϵ model may contribute to errors in the predicted flowfield, particularly the turbulence stresses. A modification to the eddy viscosity model aimed at correcting this may be a fruitful area of future study. On the other hand, Fig. 7 shows that the flow tends to approach isotropy in the dome recirculation region and in the region of $X^* \geq 4$.

Reynolds Stresses and Turbulence Kinetic Energy

The dimensionless Reynolds stresses and two-component turbulent kinetic energy of selected X^* are shown in Fig. 8. To obtain the Reynolds stresses using a single component LDV, measurements of velocity fluctuations at ±45 deg were conducted.[17-19] The measured turbulent kinetic energy was defined as $k = (u'^2 + v'^2)/2$ in view of $u' \neq v'$ for anisotropic turbulence reported in the previous section and the inability of measuring Z-component velocity fluctuations using the present LDV system. Various definitions of k can be found in Refs. 17 and 20. The maximum values of the Reynolds stresses and the turbulent kinetic energy are found in each X^* station in the region where the velocity gradient is close to a maximum (Fig. 3). This coincidence is consistent with the proposal that the Reynolds stress is proportional to the turbulent kinetic energy and mean-velocity gradients. In addition, the turbulent kinetic energy is produced by working Reynolds stresses against mean-velocity gradients. Therefore, for a given mean-velocity gradient, regions of high turbulent kinetic energy exist when high shear stresses exist. The mean velocity gradients at the centerline are nearly zero due to the approximately symmetric mean-velocity profiles (Fig. 3), and the corresponding Reynolds stresses are almost zero (Fig. 8) by definition. However, the turbulent kinetic energy is not zero along the centerline, since the corresponding turbulence intensities are not zero (Fig. 7). The Reynolds stress data are missing for $X^* = 1.1$ in Fig. 8, since one of the laser beams was blocked by the flange of the test section when measurements of velocity fluctuations at ±45 deg were conducted.

The steep gradients of mean velocity occur mainly in the jet impingement zone (Fig. 3, $0 \leq X^* \leq 1.1$) and in the shear layers of the secondary recirculation zones. The measured Reynolds stresses in these zones are, therefore, considerably higher than in the dome recirculation zone and in the zone far downstream ($X^* \geq 4$), where $\overline{u'v'}/U_{REF}^2$ is typically 10^{-3} to 10^{-4}, which is comparable to those found in fully developed rectangular duct flow.[21] The maximum values of $\overline{u'v'}/U_{REF}^2$ measured in the impingement zones and in the shear layers of the secondary recirculation zones are approximately 0.037 and 0.079, respectively. The behavior of the peak shear stress of 0.079 occurring near reattachment ($X^* = 1.6$) is in agreement with the observations of Tani et al.[22] and Bradshaw and Wang[23] for typical reattaching flows.

Effect of Dome Height

The effect of varying dome height on the time-averaged impingement stagnation point and on the time-averaged reattachment lengths was investigated. Both the impingement stagnation point and the reattachment points are found to be relatively insensitive to variations in dome height. This insensitivity may be due to the relatively strong secondary recirculation zones located immediately downstream of the inlets,

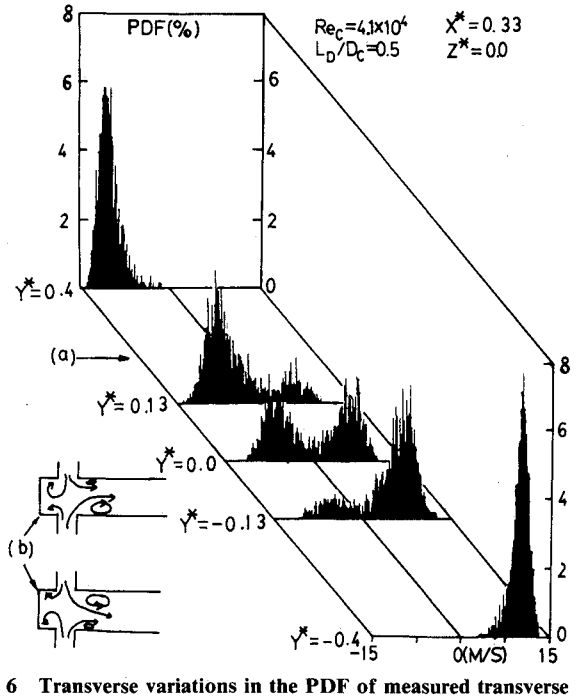

Fig. 6 Transverse variations in the PDF of measured transverse velocity at $X^* = 0.33$.

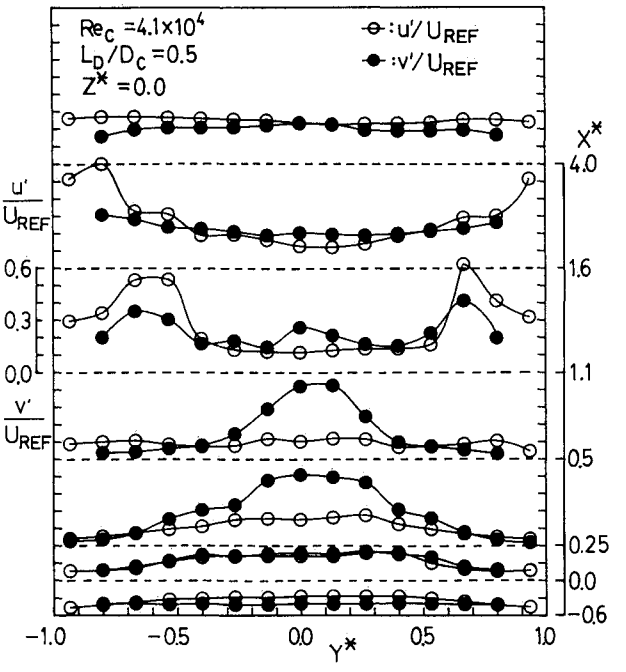

Fig. 7 Measured axial and transverse turbulence intensity profiles.

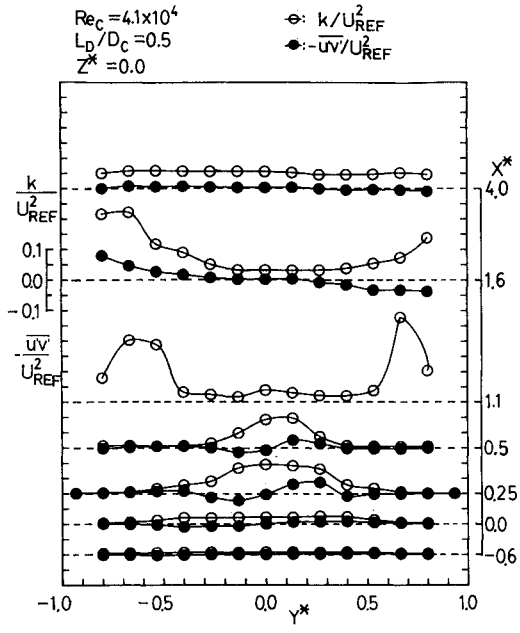

Fig. 8 Measured shear stress and turbulent kinetic energy profiles.

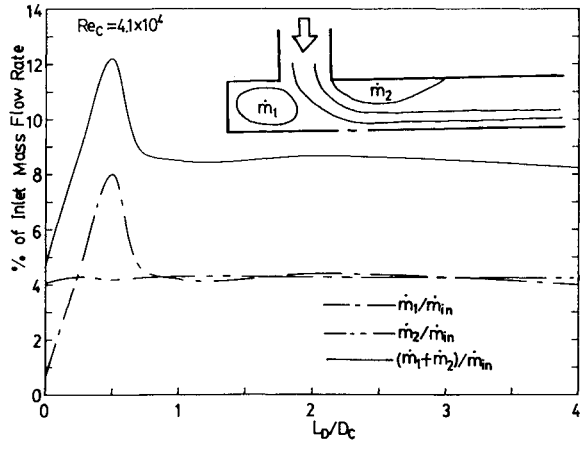

Fig. 9 Effect of dome height on $\dot{m}_1/\dot{m}_{in}$, $\dot{m}_2/\dot{m}_{in}$, and $(\dot{m}_1+\dot{m}_2)/\dot{m}_{in}$.

which are nearly independent of the increased length of the dome region where both the mean velocity and turbulence intensity are very low, as shown in Figs. 3 and 7. Hence, the impinging jets are bifurcated approximately at the same point, and the sizes of the secondary recirculation zones remain invariant to changes in the dome height. This observation suggests that the overall flowfield downstream of the impingement dividing streamline is relatively unaffected by the variation of the dome height. A similar trend was also qualitatively obtained by Stull et al.[2] using water flow visualization and theoretically predicated by Vanka et al.[4] for a three-dimensional side-dump combustor with 45-deg entry dual-inlet ducts.

Since the fraction of the inlet mass flow rate that is transported into the dome ($\dot{m}_1/\dot{m}_{in}$) and secondary ($\dot{m}_2/\dot{m}_{in}$) recirculation zones may have an important effect on the fluid mixing and the flame stability limits inside a ramjet combustor,[1] calculations of $\dot{m}_1/\dot{m}_{in}$, $\dot{m}_2/\dot{m}_{in}$ and $(\dot{m}_1+\dot{m}_2)/\dot{m}_{in}$ as functions of normalized dome height were performed, and the results are shown in Fig. 9. As one can see, the calculated $\dot{m}_2/\dot{m}_{in}$ is practically independent of the dome height. This result is a further justification of the aforementioned insensitivity of the impingement stagnation point and the reattachment lengths to the changes in the dome height. By contrast, $\dot{m}_1/\dot{m}_{in}$ first increases to a peak value of 8% as the dimensionless dome height L_D/D_C is increased from 0 to 0.5, it subsequently decreases as L_D/D_C is further increased, and then remains approximately constant for $L_D/D_C \geq 0.75$. Also, as the dome height is increased, the size of the dome region and, thus, $\dot{m}_1/\dot{m}_{in}$, increases. The presence of $(\dot{m}_1/\dot{m}_{in})_{max}$ at $L_D/D_C = 0.5$ may be due to the fact that only for $L_D = D_C/2$ the dome vortex tends to form a smooth circle that can be most easily driven by the inlet jet. Figure 9 further shows $\dot{m}_1/\dot{m}_{in} \approx \dot{m}_2/\dot{m}_{in}$ at $L_D/D_C = 0.75$, which suggests that the mass flow rates in the two recirculation zones are in equilibrium. The equilibrium condition tends to be maintained for $L_D/D_C > 0.75$ if the flowfield is steady. $\dot{m}_1/\dot{m}_{in} \approx \dot{m}_2/\dot{m}_{in}$ may indicate the possibility of attaining a more uniform energy release or temperature distribution in the combustor. $(\dot{m}_1+\dot{m}_2)/\dot{m}_{in}$ and $\dot{m}_1/\dot{m}_{in}$ have similar behavior since $\dot{m}_2/\dot{m}_{in}$ is quite insensitive to the dome height.

The variation of $\dot{m}_1/\dot{m}_{in}$ with L_D/D_C shown in Fig. 9 may qualitatively explain the computational results of Vanka et al.[4] regarding the effect of the dome height on the combustion efficiency. The calculations of Vanka et al.[4] show that $L_D/D_C = 0.38$ offers the best combustion efficiency compared with $L_D/D_C = 0$, 0.17, and 0.76. This comparison suggests the presence of a correlation between $\dot{m}_1/\dot{m}_{in}$ and the combustion efficiency.

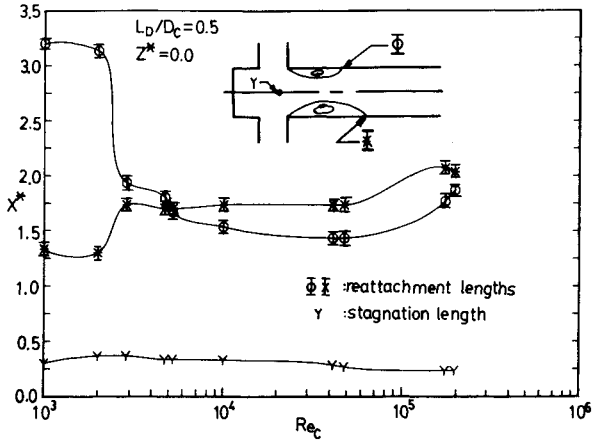

Fig. 10 Measured impinging stagnation point and reattachment points vs Reynolds number.

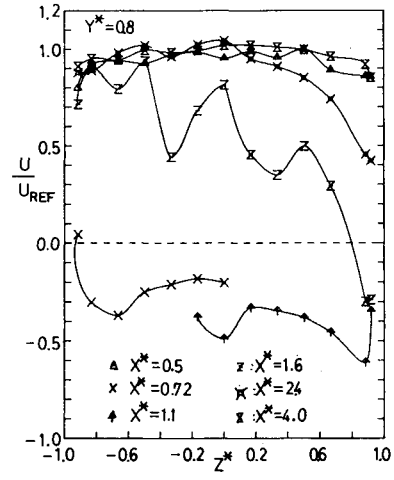

Fig. 11 Spanwise mean axial velocity profiles at various axial stations.

Effect of Reynolds Number

The data presented above are for $Re_C = 4.1 \times 10^4$. Results for other Reynolds numbers are shown in Fig. 10 in terms of

both impinging stagnation point and reattachment lengths of Re_C from 1.0×10^3 to 2.0×10^5. The impingement stagnation point is quite insensitive to the Reynolds number. However, there exists a clear transition of the reattachment lengths at about $Re_C = 2900$. For $Re_C \leq 2900$, the large difference in the reattachment lengths between the top and bottom walls reveals the asymmetrical nature of the flow. This asymmetry may be due to the instabilities of the detached shear layers shedding from the downstream edges of the inlet dump planes (i.e., $X^* = 0.5$ and $Y^* = \pm 1$), as found in coaxial-dump combustors.[24] Figure 10 indicates that the reattachment lengths remain approximately constant for $Re_C \geq 2900$ compared with $Re_C < 2900$. This trend parallels well-known results: for all Reynolds numbers sufficient to give turbulent boundary layers at the inlet, the reattachment length of the flowfield in a suddenly enlarged axisymmetric duct is a rather weak function of the Reynolds number.[25]

Spanwise Flow Distribution

The present experimental investigations were undertaken in a rectangular combustor with a cross-section aspect ratio of 4:1. All the experimental results presented earlier were measured along the center plane $Z^* = 0$. It is, therefore, important to look at the spanwise flow distribution. The spanwise mean transverse velocity profiles in the dump plane ($Y^* = 1.0$) are found to be two-dimensional over at least the center 60% of combustor width to within 2.8%. Inside the combustor, however, considerable nonuniformity in the spanwise mean axial velocity profiles is found for X^* between 0.5 and 4.0, where spanwise vortices, as found in the sudden expansion duct flow,[26] appear at $X^* = 0.72$ and 1.6, as shown in Fig. 11. Hence, the flow has a three-dimensional nature between $X^* = 0.5$ and 4.0. The three-dimensional behavior of the flow suggests that a three-dimensional computational code should be developed in order to achieve a better agreement with the measured data.

The spanwise mean transverse velocity profiles in the impingement region ($X^* = 0.28$, $Y^* = 0.0$) also provide useful information for studying the impingement of counter jets. Figure 12 shows that the jet impingement generates four to five counter-rotating vortices with their axes parallel to the combustor axis. According to the flow-visualization study by Nosseir and Behar,[5] these vortices are generated due to the out-of-phase modulation in the velocity profiles of the impinging jets.

The suitability of the two-dimensional assumption made in the present computations can be checked from a mass continuity standpoint. Two calculations were performed. One calculated the mass flow rate by integrating the experimental mean axial velocity profile over the entire combustor cross section at several measurement stations, whereas the other calculated the mass flow rate by integrating the experimental profiles along plane $Z^* = 0$ only (i.e., based on two-dimensional assumption). The results showed that the mass flow rate obtained from the former calculation is satisfactorily conserved within 5% of the inlet mass flow rate. However, the latter calculation results in a deviation as high as 23.6% from the inlet mass flow rate. This comparison is a further illustration of the need of three-dimensional simulations and may partly explain the discrepancies between measured and predicted profiles shown in Figs. 3 and 4, since the theoretically computed mean axial velocity profiles, although two-dimensional, are mass-conserving.

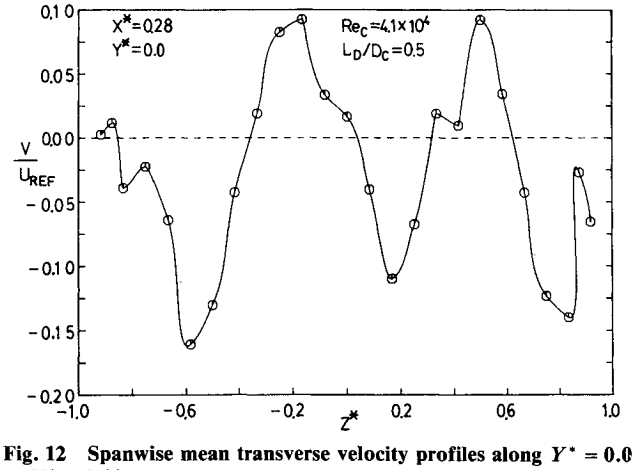

Fig. 12 Spanwise mean transverse velocity profiles along $Y^* = 0.0$ at $X^* = 0.28$.

Conclusions

The following conclusions are drawn from the data presented:

1) The anisotropic turbulence ($0.5 < X^* < 4$) found in the present study suggests that a modification to the isotropic eddy viscosity assumption used in the k-ϵ model may be a fruitful area of study.

2) Characteristics such as the insensitivity of the reattachment lengths to the dome height, the presence of a critical Reynolds number below which the flow assumes a highly asymmetric form, and the occurrence of the asymmetric velocity profiles in spite of symmetric inlet velocity profiles and symmetric test-section geometry are useful tests of computational models.

3) Both the measured spanwise flow distribution and the mass-continuity check suggest that to achieve a better prediction, a three-dimensional computer code should be developed in the future work.

The time-averaged analysis has been used in the present study and in all the previous computations[2-4] and LDV measurements[1,8] of the flowfields in side-inlet dump combustors. However, the large-scale oscillations visualized by Nosseir and Behar[5] and Miau and Sun[6] and displayed in the present study in terms of measured velocity PDF with bimodal shapes suggest that, in future investigations, additional instruments and software should be developed to perform the conditional sampling or to decompose the flowfield into a sum of mean, periodic, and random velocity components.[27]

References

[1]Shahaf, M., Goldman, Y., and Greenberg, J. B., "An Investigation of Impinging Jets in Flow with Sudden Expansion," *Proceedings of the 22nd Israel Annual Conference on Aviation and Astronautics,* Israel Ministry of Transport, Haifa, Israel, March 1980, pp. 100-106.

[2]Stull, F. D., Craig, R. R., Streby, G. D., and Vanka, S. P., "Investigation of a Dual Inlet Side Dump Combustor Using Liquid Fuel Injection," AIAA Paper 83-0420, Jan. 1983.

[3]Vanka, S. P., Stull, F. D., and Craig, R. R., "Analytical Characterization of Flow Fields in Side Inlet Dump Combustors," AIAA Paper 83-1399, June 1983.

[4]Vanka, S. P., Craig, R. R., and Stull, F. D., "Mixing, Chemical Reaction and Flow Field Development in Ducted Rockets," AIAA Paper 85-1271, July 1985.

[5]Nosseir, N. S. and Behar, S., "Characteristics of Jet Impingement in a Side-Dump Combustor," *AIAA Journal,* Vol. 24, Nov. 1986, pp. 1752-1757.

[6]Miau, J. J. and Sun, D. J., "Visualization of Impinging Flow in a Side-Inlet Square Duct," AIAA Paper 88-0502, Jan. 1988.

[7]Liou, T.-M. and Wu, S. -M., "Application of Laser Velocimetry to the Curved Inlet Duct of a Side Dump Combustor," *Third International Symposium on Application of Laser-Doppler Anemometry to Fluid Mechanics,* Ladon-Instituto Superior Technico, Lisbon, Portugal, July 1986, pp. 9.3.1-9.3.6.

[8]Liou, T.-M. and Wu, S.-M., "Flowfield in a Dual-Inlet Side-Dump Combustor," *Journal of Propulsion and Power,* Vol. 4, Jan.-Feb. 1988, pp. 53-60.

[9]Launder, B. E. and Spalding, D. B., "The Numerical Computation of Turbulent Flows," *Computer Methods in Applied Mechanics and Engineering,* Vol. 3, 1974, pp. 269-289.

[10]Patankar, S. V. and Spalding, D. B., "A Calculation Procedure for Heat, Mass and Momentum Transfer in Three-Dimensional Parabolic Flows," *International Journal of Heat and Mass Transfer,* Vol. 15, Sept. 1972, pp. 1787-1806.

[11]Drain, L. E., *The Laser Doppler Technique,* Wiley, New York, 1980, pp. 136–145.

[12]Buchhave, P., George, W. K., Jr., and Lumley, J. L., "The Measurement of Turbulence with the Laser-Doppler Anemometer," *Annual Review of Fluid Mechanics,* Vol. 11, 1979, pp. 443–503.

[13]McLaughlin, D. K. and Tiederman, W. G., "Biasing Correlation for Individual Realization of Laser Anemometer Measurements in Turbulent Flows," *The Physics of Fluids,* Vol. 16, Dec. 1973, pp. 2082–2088.

[14]Leschziner, M. A. and Rodi, W., "Calculation of Annular and Twin Parallel Jets Using Various Discretization Schemes and Turbulence-Model Variations," *Journal of Fluids Engineering,* Vol. 103, June 1981, pp. 352–360.

[15]Kennedy, J. B., "Ramburner Flow Visualization Studies," *Proceedings of 11th JANNAF Combustion Meeting,* Publication 261, Vol. II, Chemical Propulsion Information Agency, Laurel, MD, Oct. 1974, pp. 415–440.

[16]Wygnanski, I. and Fiedler, H., "Some Measurements in the Self-Preserving Jet," *Journal of Fluid Mechanics,* Vol. 38, Sept. 1969, pp. 577–612.

[17]Yang, B. T. and Yu, M. H., "The Flowfield in a Suddenly Enlarged Combustion Chamber," *AIAA Journal,* Vol. 21, Jan. 1983, pp. 92–97.

[18]Fujii, S., Gomi, M., and Eguchi, K., "Cold Flow Tests of a Bluff-Body Flame Stabilizer," *Journal of Fluids Engineering,* Vol. 100, Sept. 1978, pp. 323–332.

[19]Leder, A., "Physical Properties of Separated Flows Behind Two-Dimensional Bluff Bodies in Uniform Flows," *International Symposium on Laser Anemometry,* The American Society of Mechanical Engineers, New York, Nov. 1985, pp. 273–280.

[20]Durst, F., Founti, M., and Obi, S., "Experimental and Computational Investigaton of the Two-Dimensional Channel Flow over Two Fences in Tandem," *Third International Symposium on Applications of Laser Anemometry to Fluid Mechanics,* Ladon-Instituto Superior Technico, Lisbon, Portugal, July 1986, pp. 2.5.1–2.5.8.

[21]Gessner, F. G. and Jones, J. B., "On Some Aspect of Fully-Developed Turbulent Flow in Rectangular Channels," *Journal of Fluid Mechanics,* Vol. 23, Pt. 4, Dec. 1965, pp. 689–713.

[22]Tani, I., Iuchi, M., and Komoda, H., "Experimental Investigation of Flow Separation Associated with a Step or a Groove," *Aeronautical Research Institute,* Tokyo, Rept. 364, Aug. 1961.

[23]Bradshaw, P. and Wang, F. Y. F., "The Reattachment and Relaxation of a Turbulent Shear Layer," *Journal of Fluid Mechanics,* Vol. 52, Pt. 1, March 1972, pp. 113–135.

[24]Cherdron, W., Durst, F., and Whitelaw, J. H., "Asymmetric Flow and Instabilities in Symmetric Ducts with Sudden Expansions," *Journal of Fluid Mechanics,* Vol. 84, Pt. 1, Jan. 1978, pp. 13–31.

[25]Moon, L. F. and Rudinger, G., "Velocity Distribution in an Abruptly Expanding Circular Duct," *Journal of Fluids Engineering,* Vol. 99, March 1977, pp. 226–230.

[26]Abbott, D. E. and Kline, S. J., "Experimental Investigation of Subsonic Turbulent Flow over Single and Double Backward Facing Steps," *Journal of Basic Engineering,* Sept. 1962, pp. 317–325.

[27]Kovasznay, L. S. G., "Hot Wire Investigation of the Wake Behind Cylinders at Low Reynolds Numbers," *Proceedings of the Royal Society of London, Series A,* Vol. 198, London, Oct. 1949, pp. 174–190.